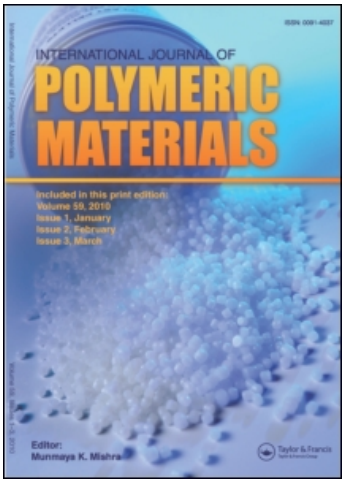

International Journal of Polymeric Materials
Publication details, including instructions for authors and subscription information:
http://www.informaworld.com/smpp/title~content=t713647664

Small Angle X-Ray Scattering of Segmented Block Copolyetheresters during Stretching

N. Stribeck[a]; A. A. Apostolov[b]; H. G. Zachmann[a]; C. Fakirov[c]; M. Stamm[c]; S. Fakirov[bd]
[a] Institut für Technische und Makromolekulare Chemie, Universität Hamburg, Hamburg, Germany [b] Laboratory on Structure and Properties of Polymers, Sofia University, Sofia, Bulgaria [c] Max-Planck-Institut für Polymerforschung, Mainz, Germany [d] Department of Chemical Engineering, Polymer Research Center and TUBITAK Advanced Polymeric Materials Research Center, Bogazici University, Istanbul, Turkey

To cite this Article Stribeck, N. , Apostolov, A. A. , Zachmann, H. G. , Fakirov, C. , Stamm, M. and Fakirov, S.(1994) 'Small Angle X-Ray Scattering of Segmented Block Copolyetheresters during Stretching', International Journal of Polymeric Materials, 25: 3, 185 — 200
To link to this Article: DOI: 10.1080/00914039408029337
URL: http://dx.doi.org/10.1080/00914039408029337

Intern. J. Polymeric Mater., 1994, Vol. 25, pp. 185–200
Reprints available directly from the publisher
Photocopying permitted by license only

Printed in Malaysia

Small Angle X-Ray Scattering of Segmented Block Copolyetheresters during Stretching

N. STRIBECK†, A. A. APOSTOLOV§, H. G. ZACHMANN†, C. FAKIROV‡, M. STAMM*‡ and S. FAKIROV||¶

†*Institut für Technische und Makromolekulare Chemie, Universität Hamburg, 20146 Hamburg, Germany*
‡*Max-Planck-Institut für Polymerforschung, Postfach 3148, 55021 Mainz, Germany*
§*Laboratory on Structure and Properties of Polymers, Sofia University, 1126 Sofia, Bulgaria*
||*Bogazici University, Department of Chemical Engineering, Polymer Research Center and TUBITAK Advanced Polymeric Materials Research Center, 80815 Bebek, Istanbul, Turkey*

(Received September 27, 1993)

The scattering behaviour of polyetherester thermoplastic elastomers based on polybutylene terephthalate as hard segments and polyethylene glycol ($\bar{M}_n$ = 1000) as soft segments in a ratio 49/51 wt.% is studied under stress. Drawn (λ = 5) bristles are annealed with fixed ends in order to create a standard initial structure. Samples with structure destroyed by additional drawing as well as with structure regenerated by solid-state reactions or chemical crosslinking are prepared. The data from small-angle x-ray scattering (SAXS) taken under or without stress are evaluated using Stribeck's method and the sizes of crystalline ($\bar{d}_1$) and amorphous ($\bar{d}_2$) regions are directly obtained. A constant value of $\bar{d}_1 \approx 50$ Å is found for all samples except for the chemically crosslinked one, for which $\bar{d}_1$ changes at deformations higher than 80% due to axial displacement of the crystallites. The size of the amorphous regions $\bar{d}_2$ measured under stress ($\varepsilon > 30$–50%) rises slightly and reversibly followed by a drop similarly to the measurements without stress, thus indicating that the observed changes in the $\bar{L}$-value are due to changes in the amorphous regions only. Further, in the chemically crosslinked sample a reversible axial displacement of the crystallites is observed in the range ε = 100–200%, suggesting a complete elimination of the interfibrillar contacts as well as stretching and relaxation of intrafibrillar tie molecules.

KEY WORDS Thermoplastic elastomers, block copolymers, SAXS, long spacing, relaxation

INTRODUCTION

Thermoplastic elastomers are generally prepared from two types of long chain segments. One of the blocks is distinguished by low melt and glass transition temperatures, the other one undergoes aggregation or crystallization, forming rigid physical crosslinks. Since some of these new materials represent block copolymers of randomized hard and soft segments, they offer a combination of resistance and strength that have never been obtained in any thermoplastic. As far as the "points" of crosslinking represent rather large aggregates, in contrast to classical rubbers, the mechanical properties of these materials depend not only on the molecular

* To whom correspondence should be addressed.
¶Permanent address: Laboratory on Structure and Properties of Polymers, Sofia University, 1126 Sofia, Bulgaria.

features and block characteristics but also on the texture of the rigid aggregates. For this reason such a basic question as the nature of the elastic behaviour of the thermoplastic materials is still open.[1]

In a thorough study on chain conformation in block copolymers by small angle neutron scattering (SANS) Miller and Cooper[2] investigated the deformation response of the polyether soft segments in polyetherester (PEE) based on polybutylene terephthalate (PBT) and polytetramethylene oxide (PTMO) with composition close to 1:1. They report that the deformation behaviour of this isotropic PEE up to stretching of $\lambda = 3$ disobeys any of the three common models, namely the affine deformation model, the junction affine deformation model and the phantom network model. Further, they evaluated the radius of gyration of the soft segments at room temperature of 12.8 Å and concluded that the majority of soft segments are in a random coil conformation and only a number of them are fairly elongated.[2]

The relationship between the macro- (external) deformation ε and the microdeformation (on morphological level expressed by the long spacing $\bar{L}$) on drawn ($\lambda = 5$) PEE based on PBT and polyethylene glycol (PEG) was recently studied by means of small angle x-ray scattering (SAXS).[3,4] It was found that the long spacing $\bar{L}$ increases linearly with the relative deformation up to $\varepsilon = 100\%$ which is explained by the reversible deformation of the amorphous regions; further rise of ε leads to elimination of interfibrillar contacts and as a result relaxation of some microfibrils occurs, leading to a second long spacing with value close to that of the initial $\bar{L}$. In order to demonstrate the essential role of the intra- and mostly interfibrillar tie molecules in the deformation and relaxation process, experiments with samples with largely destroyed structure (by additional drawing) as well as with regenerated structure (by solid state reactions or chemical crosslinking) were carried out.[5] As a result two concepts were proposed: (i) microfibrillar chemical healing—elimination of the interfibrillar phase boundaries (created during additional drawing) as a result of solid state reactions and (ii) deformation (by slippage) of ensembles of microfibrils in the chemically crosslinked samples. Finally, the observed reversible morphological transition from zigzag to smooth lamellar stacks suggests some contribution of morphology to the reversibility of the macrodeformation of thermoplastic elastomers.[6]

The above described SAXS measurements suffer the following shortcomings: (i) the $\bar{L}$-values are averaged ones and their distribution is unknown; (ii) the sizes of the crystalline and amorphous regions can be obtained only indirectly, i.e. by a combination with another experimental technique. These disadvantages can be overcome using the recently developed data analysis method[7–11] based on the Ruland's IDF theory,[12] which allows the direct evaluation of these sizes and their distribution. One-dimensional lamellar stacks are considered as a region of coherent scattering where the various sizes d_i (lamellae thickness, interlamellar distance, long spacing, etc.) are not fixed, but obey Gaussian distributions. The root mean-square variance (r.m.s.v.) of the distribution σ represents the width of the distribution curve. The relative fraction of the domains, having a certain thickness, can be found by integration of the distribution curve within the respective limits. Thus, by analysis of SAXS curves only, the parameters of the distribution d_i, σ_i, having

found physical meaning can be obtained. Various models for the paracrystalline structure can be applied in this analysis, depending on the choice of the independent parameters of the distribution.

It is the aim of this work to evaluate the above discussed SAXS data by means of Stribeck's method[10] in order to obtain direct and more precise information on the sizes of the crystalline and amorphous regions and their distributions, contributing to the deeper understanding of the peculiarities of the deformation of thermoplastic elastomers.

THEORETICAL CONSIDERATIONS

From any SAXS pattern with fiber symmetry it is possible to compute a one-dimensional (1D) scattering curve I_1, which is related to only the variations of the electron density ρ in one direction, i.e. usually the fiber direction. This computation is carried out by projecting the scattering intensity, present as the recorded 2D pattern, onto the axis of its rotational symmetry.

If the structure of the sample can be approximated by the assumption of a two phase system, I_1 is fully determined by the distribution and the arrangement of only those chord lengths, which are oriented parallel to the fiber axis. The frequency distribution of chord lengths of "phase 1" shall be denoted as h_1, the frequency distribution of "phase 2" shall be written h_2.

By identifying those frequency distributions of chord lengths with some thickness distribution of lamellae, we assume that the structure of the sample may be described by an ensemble of lamellar stacks, for which the direction normal to the lamellar surfaces is parallel to fiber direction. If $\bar{d}_1$ and $\bar{d}_2$ are the mean thicknesses of the two phases differing in their electron densities, the mean long spacing $\bar{L}$ is:

$$\bar{L} = \bar{d}_1 + \bar{d}_2 \tag{1}$$

Let $h_1(d_1)$ be the density of the probability the thickness of phase 1 to be in the interval $(d_1, d_1 + \Delta d_1)$. One can assume Gaussian distribution of the thicknesses d_1[10]:

$$h_1(d_1) = \frac{1}{\sigma_1\sqrt{2\pi}} \exp\left[-\frac{(d_1 - \bar{d}_1)^2}{2\sigma_1^2}\right] \tag{2}$$

After having defined the frequency distribution of lamellae thickness, we have to deal with their arrangement along the fiber direction. In this study we use both the "paracrystalline stacking model," which has been discussed first by Zernicke and Prins,[13] and the "paracrystalline lattice model," which is a variation of the first one. Both models have been discussed by a great number of authors.

Regardless whatever model is chosen, a weighting parameter has to be fitted during the regression process. For fits on SAXS data from a two-phase system it is obvious,[10] that this parameter is Porod's asymptote, A_p, the constant which governs the decrease of the scattering intensity according to the Porod's law.

If one applies the paracrystalline stacking model and carries out a fit, one will determine values for the model parameters $\bar{d}_1$ and $\bar{d}_2$ (the average thicknesses of the two phases) as well as the relative mean square variances of their distributions $\sigma_1/\bar{d}_1$ and $\sigma_2/\bar{d}_2$, respectively. According to this model the thicknesses of the phases change independently, the mean long period $\bar{L}$ being related to them, according to Equation (1). The value of σ_L representing the r.m.s.v. of $\bar{L}$ depends on σ_1 and σ_2 in the following way[11]:

$$\sigma_L^2 = \sigma_1^2 + \sigma_2^2 \tag{3}$$

According to the second model, the "paracrystalline lattice" model, an a priori correlation of the repetition units is assumed, i.e. L (together with d_1) changes independently within every stack of lamellae.[10] The length of the repetition unit L fluctuates due to paracrystalline disorder. At the lattice positions so defined, particles (i.e. segments having certain lengths) are situated, their average dimension being $\bar{d}_1$. Here also the individual lengths d_1 fluctuate according to their distribution function h_1. Since particles with length d_1 are situated at the lattice positions, one can assume that $\bar{d}_1$ is decorating the lattice, i.e. $\bar{d}_1$ describes the decorating phase, while $\bar{d}_2$ describes the intermediate phase. The distribution of the long period L is represented by an expression similar to Equation (2). In the frame of this model $\bar{d}_2$ and $\sigma_2/\bar{d}_2$ are not independent and can be calculated according to Equations (1) and (4), respectively[11]:

$$\sigma_2^2 = \sigma_L^2 + \frac{\sigma_1^2}{2} \tag{4}$$

Since the entire theory of the analysis of SAXS data can be found elsewhere,[9-12] only the main evaluation steps are briefly described below:

1. Scattering data are registrated by means of a two-dimensional position sensitive detector. In the present case the detector was placed vertically, its vertical axis being s_3 (the axis of stretching as well) and its horizontal axis being s_{12}. Then the coordinates of every pixel are (s_{12}, s_3) and the corresponding intensity is $I(s_{12}, s_3)$. Corrections for the detector sensitivity, primary beam profile and background are made by standard procedures.

2. Projections of the scattering intensity $I(s)$ onto the s_3-axis are obtained as described elsewhere[10]:

$$I_1(s_3) = \sum_{k=k_{\min}}^{k_{\max}} s_{12,k} \cdot I(s_{12}, s_3) \tag{5}$$

where $(k_{\min}, k_{\max})$ is any interval which covers the scattering pattern, and s_{12} and s_3 are respectively the radial and the axial components of the scattering vector in reciprocal space:

$$|s| = \frac{2 \sin \theta}{\lambda_{Cu}} \tag{6}$$

where $\lambda_{Cu} = 1.54$ Å is the wavelength of the Cu-radiation used and θ is half of the scattering angle.

3. After multiplying $I_1(s_3)$ by s_3^3, the Porod's region $I(s_3)s^3 \approx A_p$ (Porod's constant) is found.[10] From these data the Ruland's interference function $G_1(s_3)$ is obtained by subtracting A_p from $I(s_3)s^3$ in the entire range of s_3.[12]

4. A nonlinear regression analysis of the interference function using the simplex algorithm after Caceci and Cacheris[14] is performed. As an output the regression parameters $\bar{d}_1$, $\bar{d}_2$, σ_1, σ_2 or $\bar{d}_1$, $\bar{L}_1$, σ_1, σ_L are obtained. The quality of the fit is estimated according to Draper and Smith[15] by means of correlation matrix, confidence interval for each model parameter, the residual sum of squares (RSS) and the estimated error E of the fit, evaluated according to:

$$E = \sqrt{\frac{\text{RSS}}{m(m-p)}} \tag{7}$$

where m is the number of data points and p is the number of parameters.

EXPERIMENTAL

Materials

The sample material represents PEE consisting of PBT as hard segments and PEG as soft segments in a ratio of 49/51 wt.%. The synthesis is carried out on a semicommercial scale as described elsewhere[16] using PEG-1000 with rather narrow molecular weight distribution $\bar{M}_w/\bar{M}_n = 1.3$.[3] Bristles of about 1 mm in diameter were prepared by means of melt extrusion and were drawn at room temperature on a Zwick 1464 machine with a cross-head speed of 5 mm/min until the entire sample underwent neck-formation, which corresponds to a draw ratio $\lambda = l_1/l_0 = 5$, where l_1 and l_0 are the lengths of the drawn and undrawn sample, respectively. The drawn bristles were annealed with fixed ends in vacuum at $T_a = 180$°C for 6 hours and are taken as starting material.

Samples with destroyed structure (with decreased number of tie molecules) were prepared from the starting material by additional drawing of 2.5×. The sample with structure regenerated by solid-state reactions was prepared from the material with destroyed structure through annealing at 170°C for 70 hours. Chemical crosslinking was another technique for regeneration of the structure. Details on the preparation of this sample can be found elsewhere.[5]

A description of the samples is given in Table I. It should be noted that calculations based on normal kinetics of polyester formation and ^{1}H NMR as well as ^{13}C NMR measurements lead to a degree of polymerization of the hard segments between 4.9 and 4.1, respectively, which corresponds to an average molecular weight of 1050. Assuming a total molecular weight of the copolymer of about $(2-4)\cdot 10^4$, these data suggest an average total number of blocks of about 20 in each macromolecule. For an extended chain conformation, the soft segments should have a length $l_s = 80$ Å while the length of hard segments should be $l_h = 55$ Å.

TABLE I

Degree of standard drawing λ_1, degree of additional drawing λ_2, degree of total drawing λ, annealing temperature T_a and annealing time t_a of the samples, based on 49/51 wt.% PBT/PEG-1000

No	Description	Standard treatment				Additional treatment		
		λ_1	T_a,°C	λ_2	$\lambda=\lambda_1*\lambda_2$	T_a,°C	t_a,h	Chemical crosslinking
1	Starting material	5	180	-	5	-	-	-
2	With destroyed structure	5	180	2.5	12.5	-	-	-
3	Structure regenerated by solid-state reactions	5	170	2	10	170	60	-
4	Structure regenerated by chemical crosslinking	5	150	1.5	7.5	-	-	yes

Method

An x-ray source with rotating anode and a pinhole collimation was used for the SAXS measurements. The scattering patterns were registered by a two-dimensional position-sensitive detector. The detector is filled with xenon and has a resolution of 0.2 mm in each direction. The two-dimensional patterns consist of 512 x 512 data points. Sample-to-detector distance was 80 cm. The typical recording time was between one and four hours, yielding a peak intensity of typically 200 counts. The scattering measurements under stress were performed using a frame allowing a controlled change of the sample length. Each measurement under stress was immediately followed by another one in the absence of stress, before applying the next, larger deformation. The deformation at which the measurement is carried out is denoted by $\varepsilon = [(l/l_1) - 1]100\%$, where l_1 is the initial length of the originally drawn ($\lambda = 5$) bristle and l is the length during the x-ray measurement. In order to distinguish and emphasize the deformation during SAXS measurements, this deformation is denoted by ε, in contrast to the drawing before measurements, for which we keep the more common symbol $\lambda = l_1/l_0$. In the absence of stress one obtains the residual deformation using the same notation. Since there is only negligible scattering in the equatorial direction, voids are not formed at large deformations.[3]

RESULTS

Figure 1 shows the dependence of the one-dimensional lattice parameters on the deformation ε, obtained by evaluation of the SAXS data of the starting material

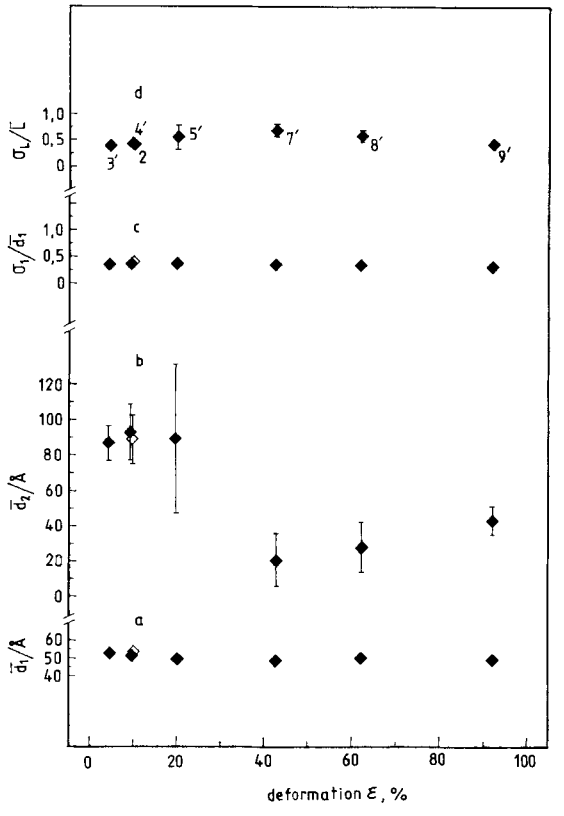

FIGURE 1 Dependence of the one-dimensional lattice parameters $\bar{d}_1$ (a), $\bar{d}_2$ (b), $\sigma_1/\bar{d}_1$ (c) and $\sigma_L/\bar{L}$ (d) (obtained by the lattice model) on the deformation ε with (◇) or without (◆) stress for the starting drawn material (sample 1, Table I). The prime sign refers to the residual deformation after the corresponding measurement under stress at deformation ε as follows (in %): 3′ - 30, 4′ - 50, 5′ - 75, 6′ - 100, 7′ - 125, 8′ - 150 and 9′ - 200. Here and further on the numbering given to curve d refers also to the rest of the points at the same deformation ε.

(sample 1, Table I) by means of the *lattice model*. First of all it should be noted that the results obtained refer only to the cases of deformation in the absence of external stress since for the measurements under stress this model does not work properly. An important observation is that $\bar{d}_1$ does not change with the deformation (Figure 1, lower curve), suggesting that $\bar{d}_1$ represents the crystallite size in the direction of the stress. This assumption is supported by our previous direct measurements of the lamellae thickness by wide-angle x-ray scattering (WAXS) leading to l_c = 55 Å.[4] Consequently, $\bar{d}_2$ refers to the amorphous domain size in the same direction. It turns out that in the absence of stress, the $\bar{d}_2$ vs. ε dependence (Figure 1, curve b) has the same trend as that established for the long spacing $\bar{L}$ of the same sample under the same conditions[3]: constant value up to a certain residual deformation, followed by an abrupt (4-fold) drop, this lower value remaining constant at higher residual deformations.

The value of r.m.s.v. of the lamellae thickness $\sigma_1/\bar{d}_1$ (Figure 1, curve c) remains constant with the deformation ε and so does (within the experimental error) the r.m.s.v. of the long period $\sigma_L/\bar{L}$ (Figure 1, curve d).

In Figure 2 the dependence of the one-dimensional lattice parameters on the deformation ε, obtained again by evaluation of the data of the starting material (sample 1, Table I) by means of the *stacking model* is shown. All four dependencies are basically the same as those shown in Figure 1. Two differences are seen: (i) the stacking model is applicable to both deformation types—under and without external stress and (ii) the root mean-square errors are larger. Furthermore, the size of the amorphous interlamellar layers $\bar{d}_2$ measured under stress shows a tendency to increase with the rise of ε up to 30% and thereafter it drops, approaching the value of $\bar{d}_2$ in the relaxed case (Figure 2, curve b).

The dependence of the one-dimensional lattice parameters on the deformation ε, obtained by evaluation of the data of the sample with destroyed structure (sample 2, Table I) by means of both the lattice and the stacking models is almost the same as that of sample 1, and for this reason it is not shown. The only difference is the lack of drop of $\bar{d}_2$ above a certain deformation. Another peculiarity is that both models are applicable to the cases with and without stress up to the maximal external deformation of $\varepsilon = 50\%$.

Figure 3 shows the dependence of the one-dimensional lattice parameters on the relative deformation ε, obtained by means of the *lattice model* for the sample with

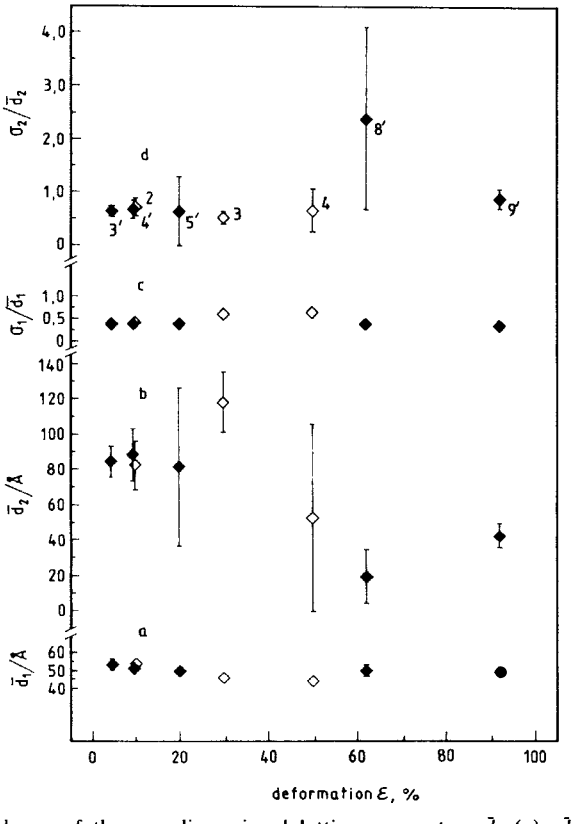

FIGURE 2 Dependence of the one-dimensional lattice parameters $\bar{d}_1$ (a), $\bar{d}_2$ (b), $\sigma_1/\bar{d}_1$ (c) and $\sigma_2/\bar{d}_2$ (d) (obtained by the stacking model) on the deformation ε under (◇) or without (◆) stress for the starting drawn material (sample 1, Table I). For the meaning of the numbers see Figure 1.

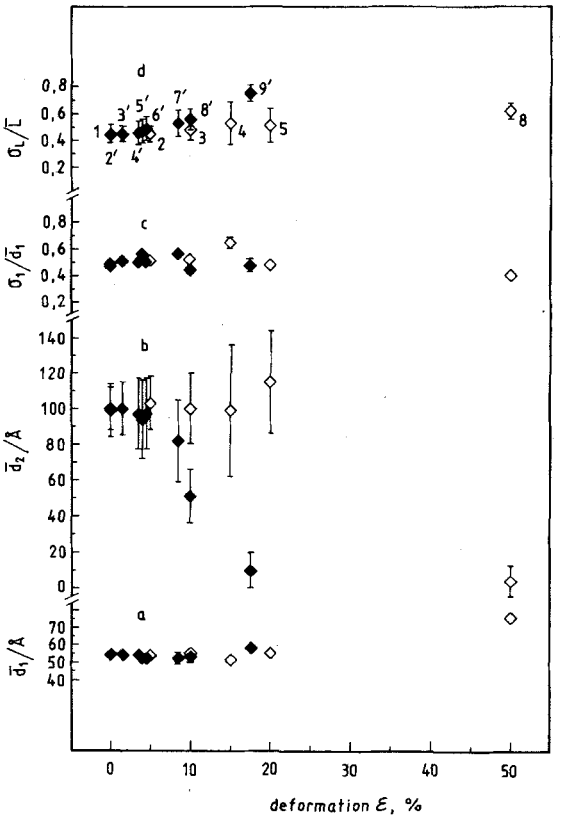

FIGURE 3 Dependence of the one-dimensional lattice parameters $\bar{d}_1$ (a), $\bar{d}_2$ (b), $\sigma_1/\bar{d}_1$ (c) and $\sigma_L/\bar{L}$ (d) (obtained by the lattice model) on the deformation ε with (◇) or without (◆) stress for the sample with its structure regenerated by solid-state reactions (sample 3, Table I). The prime sign refers to the residual deformation after the corresponding measurement under stress at deformation ε as follows (in %): 2' - 5, 3' - 10, 4' - 15, 5' - 20, 6' - 25, 7' - 30, 8' - 50 and 9' - 75.

structure regenerated by solid-state reactions (sample 3, Table I). The crystallite size $\bar{d}_1$ = 55 Å is somewhat higher than in the starting material (for which $\bar{d}_1$ = 51 Å, Figure 1, curve a) and seems to be less sensitive to ε in the deformation range up to ε = 20% (Figure 3, curve a). At ε = 50% $\bar{d}_1$ rises slightly. Although with this sample deformations under stress as high as 300% were realized, the model cannot be used for ε of more than 50%. The application of the stacking model to the same sample 3 leads to similar results (not shown) but the root mean-square errors are higher. The amorphous region size $\bar{d}_2$ derived for measurements under stress (Figure 3, curve b, open diamonds) keeps rather constant value and drops at deformations higher than ε = 50%. For the measurements in the absence of stress $\bar{d}_2$ has the same initial value and after reaching ε = 25% it smoothly drops four-fold to a value of about 10 Å. At this level (ε = 75%) the residual deformation is 18% (Figure 3, point #9').

The r.m.s.v. $\sigma_1/\bar{d}_1$ does not change with the deformation both in the presence and in the absence of stress (Figure 3, curve c). The r.m.s.v. of the long spacing

$\sigma_L/\bar{L}$ is constant when measured under stress and rises slightly with the residual deformation in the absence of stress (Figure 3, curve d, filled diamonds).

Both the lattice and the stacking model lead to rather similar results in the case of the sample with structure regenerated by chemical crosslinking (sample 4, Table I) and for this reason only the results from the application of the *lattice model* (which leads to smaller root mean-square errors of the parameters) are shown in Figure 4. A characteristic feature of this sample is that both models lead to reasonable results for all levels of deformation up to the maximal one obtained (ε = 190%) whether the measurements are carried out under or without stress. Very high residual deformation of 82% is also achieved in the absence of stress (point #11') after deformation of ε = 190% (point #11). Similar to the previous cases (Figures 1–3), $\bar{d}_1$ = 45 Å almost does not change up to ε = 80%, followed by an increase of 50% (for ε up to 150%) and with the further rise of ε $\bar{d}_1$ decreases. For the measurements without stress $\bar{d}_1$ remains constant in the entire deformation range similar to the sizes of the amorphous areas $\bar{d}_2$ (Figure 4, curve b, filled diamonds). In the measurements under stress $\bar{d}_2$ behaves rather differently (Figure

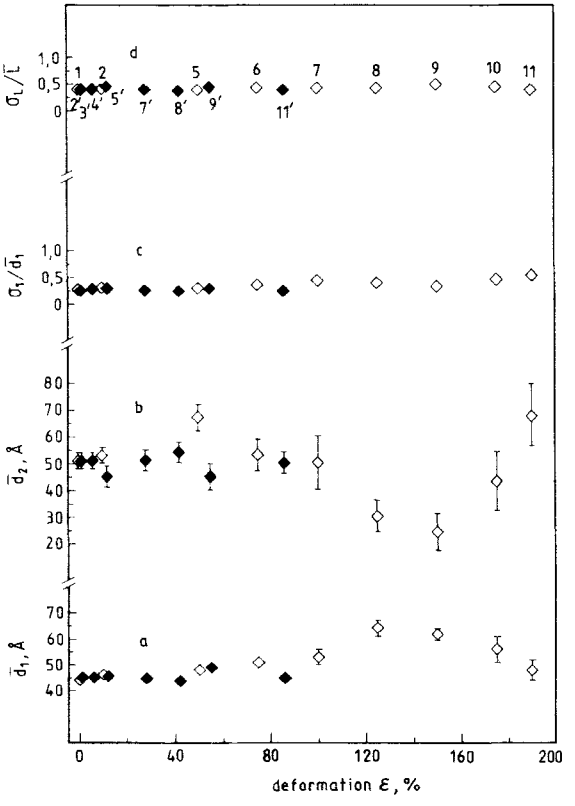

FIGURE 4 Dependence of the one-dimensional lattice parameters $\bar{d}_1$ (a), $\bar{d}_2$ (b), $\sigma_1/\bar{d}_1$ (c) and $\sigma_L/\bar{L}$ (d) (obtained by the lattice model) on the deformation ε and (◇) or without (◆) stress for the sample with structure regenerated by chemical crosslinking (sample 4, Table I). The prime sign refers to the residual deformation after the corresponding measurement under stress at deformation ε as follows (in %): 2' - 10, 3' - 20, 4' - 30, 5' - 50, 6' - 75, 7' - 100, 8' - 125, 9' - 150, 10' - 175 and 11' - 190.

4, curve b, open diamonds). Its initial value of about 50 Å drops to 25 Å in the deformation range $\varepsilon = 100-150\%$ and thereafter increases reaching the initial value at $\varepsilon = 190\%$. It should be pointed out here that this change in the size of the amorphous interlamellar layers measured under stress occurs in the same deformation range ($\varepsilon = 100-190\%$) in which just an opposite change of the lamellae thickness l_c is observed (Figure 4, curve a, open diamonds). Further, the sum $\bar{d}_2 + l_c = \bar{L}$ for each deformation step in the range $\varepsilon = 100-190\%$ is constant, suggesting some mutual compensation in the changes of $\bar{d}_2$ and l_c.

The r.m.s.v. $\sigma_1/\bar{d}_1$ in the presence of stress rises slightly with the deformation up to $\varepsilon = 190\%$ (Figure 4, curve c, open diamonds) but remains constant in the absence of stress (Figure 4, curve c, filled diamonds). This r.m.s.v. value of 0.26 is the smallest one of all four samples (Figures 1–4). The r.m.s.v. $\sigma_L/\bar{L}$ remains constant with the deformation both in the presence and in the absence of stress.

DISCUSSION

Semicrystalline polymers consist of crystalline and amorphous regions with completely different deformation ability: the crystallites undergo much less deformation than the amorphous regions. As already reported by many authors[17-19] during stretching along the fiber axis the long spacing vs. external deformation dependence is not always a linear one. From a study of the relationship between the macro- (external) deformation ε and the microdeformation (on the level of the long spacing $\bar{L}$) and a thorough survey of literature Ginzburg and Tuichiev[20] have concluded that a simple comparison of the $\bar{L}$- and ε-values does not allow to determine the mechanism of the microdeformational behaviour of oriented semicrystalline polymers. Therefore they have proposed a new approach based on the consideration of a competition between two processes taking place during uniaxial stretching of oriented polymer systems: (i) intrafibrillar deformation of long spacings and (ii) slippage of microfibrils or lamellar stacks with respect to each other.[20] SAXS measurements of various highly oriented films and fibers (including polyolefins and condensation polymers) have shown that the combination of inhomogeneous deformation of the fibrils and interfibrillar slippage may lead to different relationships between macroscopic deformation and long spacing deformation.[20] These SAXS measurements performed in a narrow range (mostly between $\varepsilon = 15\%$ and $\varepsilon = 40\%$ but not exceeding $\varepsilon = 80\%$)[20] have the same shortcomings as ours—no direct determination of the sizes of the crystalline and amorphous regions as well as of the size distributions is possible. For this reason it looks promising to follow the relationship between the macro- and microdeformation dealing with directly measured dimensions of amorphous and crystalline regions and thus getting a better understanding of the deformation mechanism.

Mechanism of Deformation of Crystalline and Amorphous Regions during Stretching

A characteristic feature of all samples studied (Table I) is that the size of the crystalline lamellae $\bar{d}_1$ in the stretching direction does not depend on the external

deformation: (i) up to $\varepsilon = 100\%$ [for the samples with standard structure, (Figures 1, 2, curve a, sample 1, Table I) and destroyed one (sample 2, Table I)]; (ii) up to $\varepsilon = 50\%$ [for the sample with structure regenerated by solid state reactions (Figure 3, curve a, sample 3, Table I)] and (iii) up to $\varepsilon = 80\%$ [for the sample with structure regenerated by chemical crosslinking (Figure 4, curve a, sample 4, Table I)]. This invariance of the l_c-values is observed regardless of the type of deformation—under or without external stress (Figures 1–4). It is still more remarkable that not only the average size of the lamellae $\bar{d}_1 = l_c$ is constant in the corresponding deformation ranges, but that its distribution also remains fixed (Figures 1–4, curve c). The values of $\sigma_1/\bar{d}_1$ are close to 0.5 with exception of the last sample, whose $\sigma_1/\bar{d}_1 = 0.25$ (Figure 4, curve c). Such an invariance of the mean crystallite size l_c with respect to macrodeformation ε must be related to the much higher elastic moduli of crystallites in comparison to those of the amorphous regions. This behaviour of l_c is supported also by direct WAXS measurements of l_c of PEE with various PBT/PEG ratios.[4] Thus, it can be concluded that the changes of the $\bar{L}$-value during deformation and the connected relaxation process are related exclusively to the changes of the dimensions of the amorphous regions in the stretching direction.

In contrast to the crystallites the mean size of the amorphous regions in the stretching direction $\bar{d}_2$ behaves differently with the increasing deformation ε. The value of $\bar{d}_2$ depends both on the sample type and on the conditions of measurement—whether experiments are performed with or without external stress. At the lowest deformation level (ε below 20%) $\bar{d}_2$ measured under stress remains almost constant for all the samples. Thereafter a slight increase with increasing deformation up to $\varepsilon = 30–50\%$ is observed, followed by a continuous drop (2–4-fold, depending on the sample type, Figures 1–4, curve b, open diamonds). The long spacing $\bar{L} = \bar{d}_1 + \bar{d}_2$ is in good agreement with the value of L, measured previously directly on the same samples where a slight increase in the same deformation range (ε up to 20%) was found.[3,5] It turns out that this increase of $\bar{L}$ and $\bar{d}_2$, respectively, is completely reversible since the values of L[3,5] and $\bar{d}_2$ (Figures 1–4, curve b) measured without stress are the same as the initial ones. Such a behaviour of $\bar{d}_2$ proves that macrodeformation in this deformation range is related exclusively to conformational changes (stretching and relaxation) of the chains in the amorphous regions as suggested repeatedly before.[3–5,20]

The drop of $\bar{d}_2$ at macrodeformations of 30–50% or more (depending on the sample type) is due to drastic relaxation of the chains in the amorphous regions leading to a 2–4-fold decrease of the size of these regions. This behaviour of $\bar{d}_2$ proves in the best way the validity of the model suggested for the explanation of a similar drop of L-values in the same deformation range—relaxation of microfibrils as a result of elimination of interfibrillar contacts since tie molecules are pulled out.[3]

An additional proof in favour of this statement is the behaviour of $\bar{d}_2$ measured in the absence of stress—it drops 4–5 times (Figures 1–3, curve b, filled diamonds). It is worth noting here that the values of L determined using Bragg's equation[3,5] are always higher than those calculated from $\bar{L}\,\bar{d}_1 + \bar{d}_2$ in this work for both types of measurements, i.e. under and without stress.

Another striking observation is that the dimensions of the amorphous regions $\bar{d}_2$ in the relaxed state for nearly all samples (except the crosslinked one), being between 10 and 20 Å (Figures 1–3, curve b, filled diamonds), are very close to those measured by SANS on a similar PEE based on PBT and PTMO-1000. They are reported to range between 11 and 13 Å (in undrawn samples) for SANS experiments by Miller and Cooper.[2] This fact shows that stretching during the measurements up to $\varepsilon = 50\%$ of the predrawn and annealed samples (Table I, samples 1–3) leads to an almost complete elimination of the interfibrillar contacts, slippage of microfibrils and a regime where relaxations predominate. The denser packing of the chains in the relaxed amorphous regions results in higher ρ_a-value which, together with the lower ρ_c-value (due to the more defective crystalline structure after stretching), leads to a drastic drop of the scattering intensity (more than threefold) as reported earlier.[3,5] This strong decrease of the intensity leads to a corresponding decrease of signal to noise ratio, which can explain why the approach of Stribeck[10] does not work for deformations higher than $\varepsilon = 50\%$ (Figures 1–3). It may also explain the differences in L-values measured previously[3,5] and in the present study for the same samples.

The Role of the Chemical Network for the Deformation and Relaxation Processes

The deformation behaviour of the sample with structure regenerated by chemical crosslinking (Figure 4) deserves special attention since it reveals considerable differences from the other three samples. First of all the method of Stribeck[10] can be applied only for this sample in the entire deformation range ($\varepsilon = 0$–190%) for the measurements taken under stress (Figure 4, open diamonds). Second, the lamellae thickness l_c does not remain any more constant when the deformation approaches $\varepsilon = 80\%$—it rises by 50% (at $\varepsilon = 120\%$) and thereafter decreases to the starting value (at $\varepsilon = 190\%$). Also in the same deformation range the size of the amorphous region $\bar{d}_2$ goes down (again by 50%) and then up, i.e. the long spacing $\bar{L} = \bar{d}_1 + \bar{d}_2$ remains constant as it does in the previous deformation range ($\varepsilon = 0$–80%, Figure 4). Third, the size of the amorphous regions measured without stress in the range $\varepsilon = 0$–80% stays at a constant value, almost equal to that obtained from the measurements under stress.

What could be the reason for such a different behaviour of the crosslinked sample? In order to answer this question one has to remember that in agreement with these observations, the previously calculated L-values using Bragg's equation showed that the L-value measured without stress remains constant ($L = 100$ Å) in the entire deformation range while L measured under stress rises slightly by 20% in the range $\varepsilon = 0$–100% and remains constant at higher deformations.[5] Further, one has to take into account that structure regeneration causes primarily the recovery of the interfibrillar contacts to the initial level (before the destruction of the structure) and in some cases even to a higher extent by introducing new tie molecules. when chemical crosslinks are used for the regeneration of the structure a more or less dense three-dimensional network is created which obviously affects the entire deformation behaviour of the sample. Only by the existence of a rather dense network interconnecting all morphological elements (crystallites, lamellae, microfibrils) one can first explain the lack of significant elongation of the

amorphous regions during stretching (Figure 4, curve b, open diamonds) and second, what is more important, the absence of relaxation after removal of the stress (Figure 4, curve b, filled diamonds), in contrast to the previous cases (Figures 1–3). Such a behaviour of the amorphous regions suggests that no pulling out of tie molecules and subsequent slippage of microfibrils occurs in this deformation range.

In the next deformation range (ε = 100–200%) a mutual compensation of $\bar{d}_1$ and $\bar{d}_2$, i.e. $\bar{L} = \bar{d}_1 + \bar{d}_2$ = const, is observed, suggesting some morphological rearrangements. The higher stress applied causes presumably an axial displacement of crystallites in such a way that, while penetrating into the amorphous regions, they preserve the original interlamellar distance ($\bar{L}$ = const, Figure 4).[5] At the same time the lamellae thickness $\bar{d}_1$ increases and the size of amorphous regions $\bar{d}_2$ decreases, as actually observed (Figure 4, curves a and b, open diamonds). This displacement is reversible to a great extent since after removal of the stress $\bar{d}_1$ and $\bar{d}_2$ both recover their initial values (Figure 4, curves a and b, points #8′, 9′ and 11′). The observed behaviour of $\bar{d}_1$ and $\bar{d}_2$ is related to the more or less complete elimination of interfibrillar contacts as well as to stretching and relaxation of the intrafibrillar tie molecules.

Finally, another peculiarity of this sample should be mentioned—the values of $\bar{d}_1$ and $\bar{d}_2$ (in the range ε = 0–80%) as well as of $\bar{L}$ remain unchanged when the external macrodeformation amounts to ε = 190%. A possible explanation of this "contradiction" between micro- and macrodeformation represents the deformation concept of microfibrillar ensembles proposed earlier.[5] During stretching the contacts between the microfibrillar ensembles are being eliminated and their slippage results in the observed macrodeformations. At the same time the microfibrils within the ensembles remain almost unaffected and thus $\bar{L}$, $\bar{d}_1$ and $\bar{d}_2$ keep their constant initial values.

In summary it should be pointed out that the chemically crosslinked sample displays the predominant role of tie molecules in the deformation and relaxation process of these polymeric materials.

CONCLUSIONS

One-dimensional paracrystalline lattice and stacking models are successfully applied to the analysis of the lamellar morphology of PEE and its changes during deformation. Due to the poor counting statistics in the scattering patterns a more sophisticated analysis was not possible. Nevertheless, some peculiarities are found:

1. As a whole, both the lattice and the stacking models are applicable to the range of low to moderate deformations. The stacking model has less model-inherent constraints in comparison to the lattice model and for this reason is capable to describe some data sets which cannot be fitted with the lattice model. This observation is especially valid at higher deformations. In addition, the intervals of confidence for some of the parameters are considerably broader than those with the lattice model, i.e. even if data can be fitted with the stacking model, some of the parameters are not reliable.
2. In all cases both models lead to similar results and trends.

3. In some cases (mainly moderate to high deformation under stress) both models fail, probably due to the simultaneous presence of two different kinds of regions, namely strained and relaxed ones. We suppose that those more complicated structures require more sophisticated models (including two lattices), but the poor counting statistics of experimental data makes the application of such models obsolete.

4. Low and moderate macroscopic deformations lead to corresponding deformations of well-defined lamellar stacked regions, whereas at high deformations the microscopic deformation does not propagate in well-defined lamellar stacks, which contribute to SAXS.

5. Regeneration of the structure by solid-state reactions results in microfibrillar healing, i.e. reestablishment of interfibrillar contacts. At higher deformations these contacts are gradually destroyed and more fibrils relax, leading to a decrease of the size of the amorphous regions and an enlargement of the distribution of the long spacing.

6. Low and moderate macrodeformations of the sample with structure regenerated by chemical crosslinking take place through slippage of ensembles of microfibrils preserving the original sizes of the morphological elements. At high deformation axial displacement of crystallites occurs, leading to a change of $\bar{d}_1$ and $\bar{d}_2$ in a way that their sum remains constant. Dedicated data analysis techniques thus yield additional information on the morphological arrangement and chain relaxations during deformation which mostly supports previous concepts and conclusions.

Acknowledgment

It is a pleasure to acknowledge the financial support provided by NATO through grant CRG 920985 and by the Bulgarian Ministry of Education and Science. A. A. Apostolov appreciates the hospitality of the Institut für Technische und Makromolekulare Chemie der Universität Hamburg, where part of this work was carried out in the frame of the Partnership Contract between the University of Hamburg and Sofia University. The authors acknowledge also the technical help of M. Bach during the x-ray measurements at Max-Planck-Institut für Polymerforschung, Mainz.

References

1. G. Wegner, Model studies toward a molecular understanding of the properties of segmented block copolyetheresters, in Thermoplastic Elastomers (ed. by R. Legge, G. Holden and H. E. Schroeder) Carl Hanser Verlag, Munich, 1987, p. 405.
2. L. A. Miller and S. L. Cooper, Chain conformation in block copolymers by small angle neutron scattering, in Reference 1, p. 385.
3. S. Fakirov, C. Fakirov, E. W. Fischer and M. Stamm, *Polymer*, **32**, 1173 (1991).
4. A. A. Apostolov and S. Fakirov, *J. Macromol. Sci.-Phys.*, **B31**, 329 (1992).
5. S. Fakirov, C. Fakirov, E. W. Fischer and M. Stamm, *Polymer*, **33**, 3818 (1992).
6. S. Fakirov, C. Fakirov, E. W. Fischer, M. Stamm and A. A. Apostolov, *Colloid Polym. Sci.*, (in press).
7. N. Stribeck and W. Ruland, *J. Appl. Cryst.*, **11**, 535 (1978).
8. N. Stribeck, *Colloid Polym. Sci.*, **270**, 9 (1992).
9. N. Stribeck, *Colloid Polym. Sci.*, (in press).
10. N. Stribeck, *Colloid Polym. Sci.*, **267**, 301 (1989).

11. N. Stribeck, Ph.D. Thesis, Marburg, 1980, p. 55.
12. W. Ruland, *Colloid Polym. Sci.*, **255**, 417 (1977).
13. F. Zernicke and J. A. Prins, *Z. Phys.*, **41**, 184 (1927).
14. M. S. Caceci and W. P. Cacheris, *Byte*, **5**, 340 (1984).
15. N. R. Draper and H. Smith, Applied Regression Analysis, John Wiley, New York, 1966, chap. 10, p. 263.
16. S. Fakirov and T. Gogeva, *Macromol. Chem.*, **191**, 603 (1990).
17. H. Zhan and U. Winter, *Kolloid-Z.*, **128(3)**, 142 (1952).
18. K. Ishikawa, K. Miyasaka, M. Maeda and M. Yamada, *J. Polym. Sci.*, **A-2**, 7, 1259 (1969).
19. Sh. Tuichiev *et al.*, *Vysokomol. Soed.*, **Ser. B 19**, 227 (1977).
20. B. M. Ginzburg and Sh. Tuichiev, *J. Macromol. Sci.-Phys.*, **B31**, 291 (1992).